Journal of Aerosol Science 156 (2021) 105785

Contents lists available at ScienceDirect

Journal of Aerosol Science

journal homepage: http://www.elsevier.com/locate/jaerosci

A novel method to investigate detachment of particulate structures from an elastic single fiber at low gas flow velocities

Lukas Poggemann *, Jörg Meyer, Achim Dittler

Karlsruhe Institute of Technology, Institute of Mechanical Process Engineering and Mechanics, Straße am Forum 8, 76131, Karlsruhe, Germany

ARTICLE INFO

Keywords:
Elastic
Fiber
Fiber-mounting device
Detachment

ABSTRACT

The detachment of particle structures from a stiff single fiber exposed to an airflow has been investigated by (Jankowska et al., 2000; Larsen, 1958; Löffler, 1972; Przekop et al., 2004; Qian et al., 1997; Zoller et al., 2020). In order to detach particle piles from a stiff single fiber, airflow velocities above 1.2 m/s are required. While these values are well above typical operational parameter for depth filters, a shift toward lower velocities for detachment would offer both up- and downside for filter operation. One possible application for controlled structure detachment from a filter fiber at lower velocities would be a shift of separated particulate structures from the upper layers of depth filter into lower regions. The result would be additional void space from particle deposition. Currently there is no knowledge available, if fiber stretching could enable such detachment of particle structure fragments at an operation airflow velocity below 1 m/s. It is assumed that fiber stretching might introduce shear and tensile stress to the particulate structures. That may lead to first cracks and promote final detachment. This study examines the behavior of particle structure fragments on an elastic single fiber for the first time. The fiber is loaded with a compact particle structure in a loading chamber. Glass spheres served as inert particulate material. A new customized fiber-mounting device was designed for the stretching procedure of 22 mm (55%) length. In first experiments, the fiber was stretched without an airflow. Stretching at an elongation rate of 0.4 mm/s caused re-arrangement, crack formation and rotation of the fiber. No detachment of particle structure fragments is observed. If the fiber is stretched and exposed to an airflow at 0.8 m/s, particles structure fragments re-arranged and subsequently detached. In further experiments at an elongation rate of 1.2 mm/s, intensive detachment is observed at an increase of superficial airflow velocity from 0.4 m/s to 0.8 m/s. In total, this reveals that fiber stretching enables detachment of particle structure fragments from a single fiber exposed to an airflow at superficial velocities below 1 m/s. The potential application of elastic fibers in a filter system will have the aim to delay increasing filter backpressure. This effect could be caused by the transport of particulate matter towards areas of lower loading further downstream while maintaining a high level of separation efficiency at operational filtration velocities.

1. Introduction

Depth filtration is commonly used for particulate matter removal in various fields of applications such as air-conditioning and cleanroom technology. The primary factors to characterize the operational behavior of depth filters are separation efficiency, pressure

* Corresponding author.
E-mail addresses: lukas.poggemann@kit.edu, gps@mvm.kit.edu (L. Poggemann).

https://doi.org/10.1016/j.jaerosci.2021.105785
Received 10 November 2020; Received in revised form 23 January 2021; Accepted 3 March 2021
Available online 15 April 2021

drop and loading capacity (Song et al., 2006). In typical depth filters the pressure drop across the filter system rises at different value with increasing deposited particulate mass in the filter medium (Payatakes und Gradoń 1980; Kanaoka und Hiragi 1990). Hence, the energy consumption is increasing, too. Fig. 1 shows an exemplary evolution of collection efficiency and pressure drop over collected particle mass. The pressure drop is generally developing through three different stages during a filtration procedure. During depth filter stage, the pressure drop is increasing slowly. In this stage, the particles are captured by the different collection mechanisms of individual fibers (Payet et al., 1992). Inside a filter, a gradual build-up of particles at the fiber surface takes place. At the end of the depth filter stage, the pressure drop is increasing slightly faster than before.

This is caused by parts of the filter where deposits on neighboring fiber at the upstream side of the filter start to form bridges. In these clogged areas, the deposition moves from the interior fibers of the filter to the deposit structure on the upstream surface. In the transition phase, more and more parts of the surface clog and at the end of this phase, the whole filter area has switched to surface filtration. Subsequently, in the final surface filtration phase, a particle layer grows on the upstream side of the filter, causing a much steeper jet linear increase in pressure drop with increasing thickness of the layer. Further, the collection efficiency reaches very high values close to 100% (Brown, 1993; Wang et al., 2016). Once the filter is clogged and transition to surface filtration occurs, the filter interior is not receiving much particles and thus, no increase in local loading. The filter stays with void space that is not filled with deposit structures, especially at the downstream parts of the filter volume (Brown, 1993).

The overall depth filter service life is determined by the development of pressure drop. In order to delay the steep, the pressure drop increase of the surface filtration stage, more void space especially at the upstream part of in the filter is needed. A chance to clear up space for new particles would be to release blocked pores in the upstream layers of the filter. One way to achieve this would be to stretch the entire filter structure or the individual fibers that make up that structure. It is assumed that stretching of a particle-loaded fiber might induce shear and tensile stress to the particulate structures in these layers. As seen in experiments and calculations by Thouless and Nahta et al., the movement/stretching of an elastic substrate beneath a coating matrix is able to induce cracks. The attached material is exposed to tensile/shear stress in a competitive process between the matrix (coating) and the substrate (fiber, elastic substrate) (Thouless, 1990). Ochai et al. and Lowden et al. have examined exemplary investigation were they observed multiple matrix cracking when subjecting a loaded/coated fiber to tensile stress. (Ochiai und Murakami 1981; Lowden und Stinton 1988)

Thus, the introduction of fibers, which are adjustable over the service of the filter, may lead to these first cracks and promote the transport/removal/detachment of particles to deeper filter layers. Clogging would be delayed. Currently, in common depth filters only stiff fibers are used.

In order to investigate the overall operating behavior of an entire depth filter with stretchable fibers, a basic visual and qualitative, and subsequently, quantitative understanding of effects of fiber stretching on particle structures on an individual stretchable fiber is needed. For this purpose, the collection behavior and detachment behavior of particle agglomerates on an isolated fiber are considered. Only when this knowledge is obtained, the results of basic single fiber experiments can be transferred to the entire fiber matrix in a filter system. An additional step might be the stretching of the entire filter structure to increase the total volume of the filter thus releasing more void space for additional particle deposition. A potential development of pressure drop for a time-adjustable fiber structure is shown in Fig. 1.

In the case of the particle detachment from stiff single fibers, numerous investigations have been carried out. Normally the mechanism of particle detachment and particle bounce occur at higher flow velocity than in the velocity range of depth filer applications (Rembor et al., 1999; R. Maus und H. Umhauer 1996).

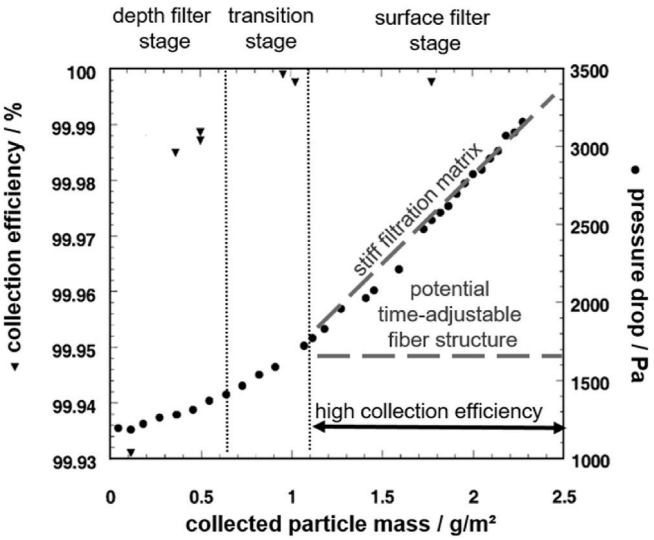

Fig. 1. Collection efficiency and pressure drop over collected particle mass of a stiff filtration matrix and of a potential time adjustable fiber structure. Modified from (Thomas et al., 2001).

Löffler (Löffler, 1972) described first investigations on the limits and conditions for detachment of individual particles and particle structure fragments from a single fiber. One main finding was that inert particles only detach from a filter fiber if flow velocity is significantly higher than common filtration velocities. In detail, Löffler distinguished between single particles with a diameter ($d_{particle}$) of 10 μm and piles consisting of particles. All particles were deposited on fibers with a diameter of (d_{fibre}) 50 μm at a filtration velocity below 0.85 m/s. For detachment of 50% of single particles, an airflow velocity of above 10 m/s was necessary. First detachment of piles of particles from the stiff fiber was observed at an airflow velocity of 1.2 m/s (Löffler, 1972).

Larsen obtains airflow velocities above 20 m/s for the detachment of 16 μm particles from a stiff fiber (Larsen, 1958). Qian et al. investigated the reentrainment of small particles (pathogens) from loaded filters. The filters were subjected to airflow higher than relevant filtration velocity and in the opposite direction of filtration flow. First detachment of particle with a size of 0.6–5.1 μm μm was observed at an airflow velocity of 0.7 m/s (Qian et al., 1997). Jankowska et al. determined a lower reentrainment for of KCL particles ($d_{particle} = 2.55$ μm and $d_{particle} = 3.25$ μm) than for fungal spores ($d_{particle} = 3.21$ μm) at the same filtration velocity of 3.00 m/s. Less than 1% of KCL particles detached at this velocity (Jankowska et al., 2000). The weakening of adhesive/cohesive strength due to chemical reactions and the followed detachment of particle structures was described by Zoller et al. (Zoller et al., 2020). They observed the detachment of glass spheres and soot from a single fiber after reaction at a flow velocity of 0.5 m/s as opposed to 1.9–2.6 m/s without reaction.

In a simulation Przekop et al. estimated the collection efficiency of particles ($d_{particle} = 0.01$–10 μm) on a single fiber. They calculated that deposition efficiency of particles on the fiber is 10–20% higher without considering the resuspension during the filtration process. Filtration velocity/face velocity in these experiments was given as 0.1 m/s (Przekop et al., 2004). This found low value in filtration velocity for detachment is an exception, but there is not a single experimental evidence for it.

In all experimental investigations, the velocities for detachment of inert particles/particle structures are rather high compared to common filtration conditions. Further, quoted investigations were focused on detachment of small amounts of particles from a stiff collector. Currently, none of this research projects considered the weakening of particle structures on the fiber due to stretching and movement of the fiber/substrate, which might cause a detachment also at low gas flow velocities.

One important decisive and influencing factor for detachment of particle structure fragments is the morphology and the shape of the particle structure (PS) on the fiber. The PS on the fiber is formed during the first stage of filtration in a fiber loading process. Starting at this point Kanaoka et al. showed that there is an influence of the filtration velocity on morphology of particulate agglomerates on a cylindrical stiff fiber.

The study examined fundamental dependencies between the filtration velocity and the different collection mechanism. Fig. 2 shows respectively a schematic of the relationship between the dimensionless numbers and the deposited structure, which were obtained by experimental and theoretical considerations. High Stokes-numbers promote a more compact structure on the front side of the fiber (highlighted in Fig. 2). Particles have large inertia and move straight to the fiber (Kanaoka et al., 1986). Based on this findings, Kasper et al. (Kasper et al., 2010) investigated the shape of the PS on the fiber that are formed under different flow conditions and with different single particle diameters. Here a high Stokes-number and low interception parameter promote rather compact structures, whereas low Stokes-number and increased interception parameters result in dendritic structures with a different/larger cross-sectional

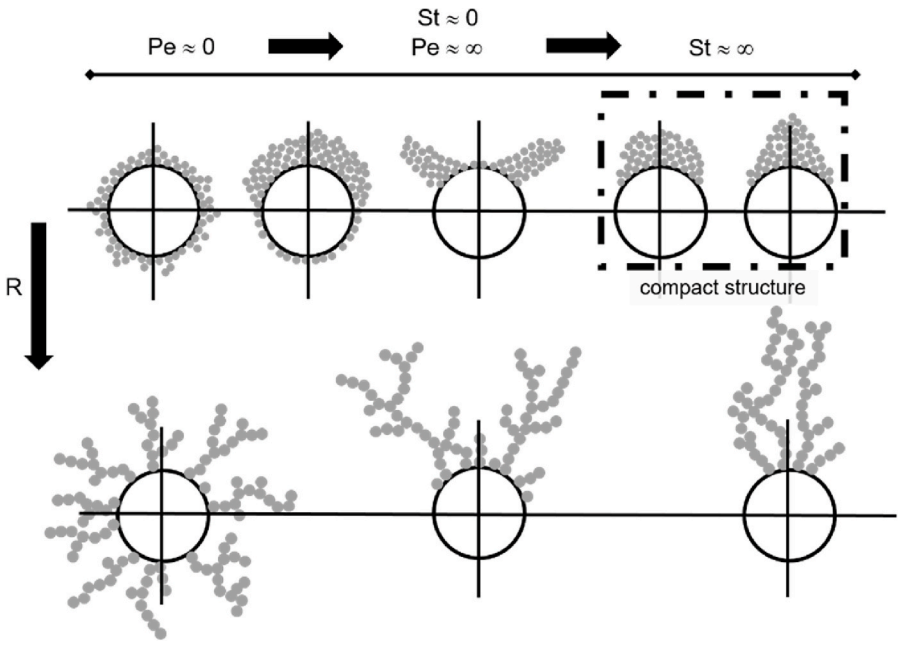

Fig. 2. Schematic relationship between the deposit structure and filtration conditions in detail of the dimensionless numbers Peclét, Stokes-number and interception parameter R. Highlighted the compact deposition morphology with higher Stokes-number. Modified from (Kanaoka et al., 1986).

area. Finally, the morphology, size and height of PS on the fiber have an influence on the drag coefficient (Müller, 2017) and consequently influence on particle detachment.

Usually the filter fiber was operating as a stiff element in the system. In order to decelerate the rise of pressure drop, it might be of high interest to generate knowledge about the detachment and cracking of PS fragments and single particles from/on a single filter fiber. In this study, the influence of fiber stretching and low airflow on the behavior of PS fragments on an elastic fiber is investigated for the first time. This initial experimental investigation demonstrates that effects like cracking and detachment of inert PS during filter fiber stretching can occur. Nevertheless, further investigations are needed concerning the detailed process conditions for breakage and detachment of PS within/from a fiber matrix. This expertise might then be used in the future to implement a component in the system adjustable over time. The aim is to clear some void space in the upstream areas of the filter, thus slowing down pressure drop increase while maintaining a high collection efficiency, as shown in Fig. 1.

2. Materials and methods

2.1. Fiber and aerosol

For all investigations, polymeric fiber made of polyurethane were used as collector. Fiber material parameters allow a temporary reversible stretching up to 75% elongation and a maximum elongation of about 300%. The elastic modulus of the fiber is measured as 0.49 MPa. In relaxed state, the fiber has an initial diameter of 82 µm in average. Stretching reduces the fiber diameter by approximately 18% at 55% elongation.

A poisson ratio of 0,327 was calculated. To avoid any contamination and surface-charge effects, the fiber was cleaned with ethanol before each loading process. Further, the fiber was handled only with tweezers and gloves during the clamping. As shown in Fig. 3 a), the fibers are entangled in their original state. Fig. 3 b) shows an SEM image of an extracted disentangled fiber, as it would be provided for the loading and stretching procedure. The unstretched state of the fiber was established by the same clamping length and the same clamping force for each fiber (here, “unstreched” refers to the initial state of the clamped fiber before particle deposition and stretching of the loaded fiber). Further, a visual inspection using the microscope was performed.

Spheriglass 5000 CP00, glass spheres made from solid soda lime A-Glass with a given material and bulk density ($\rho_{material}$ = 2.46 g/cm^3, ρ_{bulk} = 1.28 g/cm^3, $n_{refractive\ index}$ = 1.51), obtained from Potters Industry, served as the inert particulate material in all experiments. Fig. 4 a) shows the particle size distribution of the glass spheres. The size distribution was determined using laser light scattering (HELOS & RODOS, Sympatec) with a dispersion pressure of 1.0 bar (g). The average diameter was determined as $x_{50.3}$ = 7.73 µm. The particles are mostly spherical as shown in Fig. 4 b). A similar inert particulate material was used by Zoller et al. (Zoller et al., 2020)

2.2. Set-up for fiber loading process with particulate material

Fig. 5 depicts the flow diagram of the loading procedure of the fiber. In the loading procedure, the aerosol is generated using a Topas SAG 410/U as used by Zoller et al. (Zoller et al., 2020). Thereby the particulate material is dosed by a rotating ring and dispersed by an ejector nozzle (DIN ISO 5011). The particulate material was provided in a storage tank. For stable particle mass flow an ejector nozzle pressure of 1.8 bar (g) is necessary. This results in a volume flow of 23 l/min in the feed flow. A mass flow rate of Spheriglass 5000 CP00 in the feed flow (direct beyond the aerosol generator) of 4 g/h was set for the selected feeding ring speed (5% of maximum speed) and height of the scraper (5 mm). The loading time was 15 min in all experiments.

The loading equipment includes a section upstream and downstream the loading chamber. The generated aerosol feed flow is divided into loading flow ($\dot{V}_{loading}$= 14.28 l/min) for the loading chamber and excess flow ($\dot{V}_{excess}$= 8.72 l/min). The excess flow is

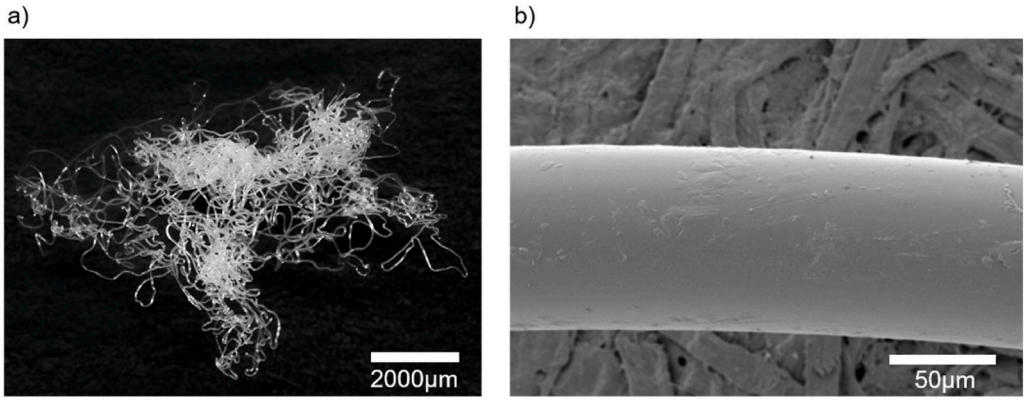

Fig. 3. a) Fiber in their original state, entangled, white polymeric structure. b) Fiber disentangled and clamped under the SEM – straightened, unstrechted with initial diameter of around 82 µm.

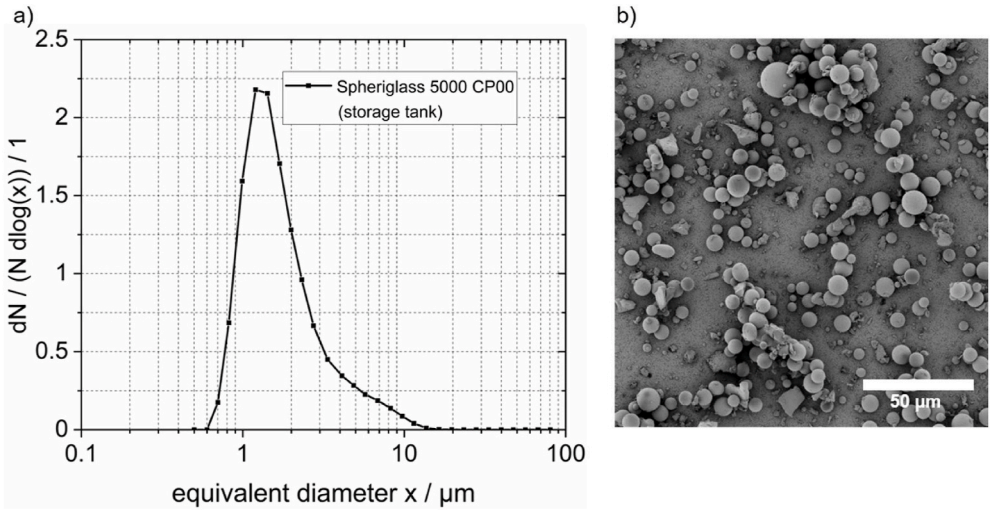

Fig. 4. a) Particle size distribution of used Spheriglass 5000 CP00 in the storage tank of the dust generator. Measured offline by HELOS & RODOS, Sympatec b) An according SEM image of the glass particles.

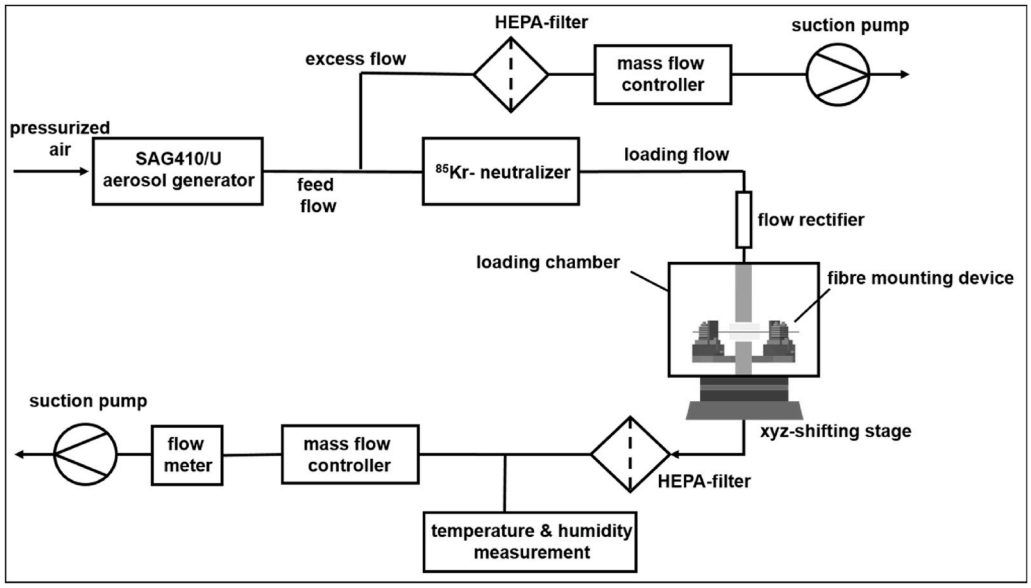

Fig. 5. Process flow diagram of the loading procedure including the fiber-mounting device.

drained off by a separate suction pump to obtain the correct stable particle mass flow in the loading flow and a stable filtration velocity applied to the fiber. The particulate material is removed by a HEPA-filter following a mass flow controller (MFC). The balance of feed flow and loading flow determines the size of excess flow.

After generation, the aerosol passes a ^{85}Kr – neutralizer to reduce the electrical charge of glass spheres. A flow rectifier is placed at the inlet of the loading chamber to establish a laminar plug flow field. The flow rectifier (tube bundle) is located in the inlet pipe, which has a diameter of 16 mm. Subsequently, in the loading chamber the flow forms a short free jet that flows around the fiber allowing particle deposition. After passing the fiber, the flow is approaching the aerosol outlet tube at the exit of the loading chamber. The loading chamber is sealed to avoid any contamination by environmental air and to establish a well-defined volume flow.

The section downstream the loading chamber consists of a HEPA-filter, various devices for flow control, measurement and a suction pump. In order to enable reliable and repeatable results, the humidity, temperature (Sensirion, SHT85) and volume flow rate (TSI, Flow Meter 4000 series) of the aerosol flow are measured after the HEPA-filter. The volume flow rate of the aerosol and thus the aerosol velocity at the fiber are adjusted by MFC. A calibration of the MFCs was regularly carried out using a bubble flow meter with a precision of 0.03 l/min. Loading procedure was performed at about 20–25 °C. Humidity of loading flow was around 10%. There was no extra differential pressure applied across the loading chamber.

As written in the introduction several deposition morphologies for PS on a single fiber are feasible. To obtain a PS on the upstream side top of the fiber a flow velocity of 1.2 m/s corresponding to Stokes-number of 3.42 was selected. Under the given circumstances, the particles mostly deposit due to inertia on the fiber.

2.3. Fiber mounting device

For controlled stretching of the elastic fiber a new fiber-mounting device was designed and built, which fits into the existing loading chamber (Schweers et al., 1994). One challenge for the new fiber-mounting device (shown in Fig. 6) emerges from the spatial confinement in the loading chamber. Further, the fibers have a maximum length of around 100 mm. The elastic fiber is fixed in the clamping system and positioned by cone-shaped boreholes of 90 μm in the 3D-printed L-section.

In order to stretch the fiber, each side of the mounting system is placed on a piezo actuator driven stage (PI, Q-521). By using two motors, which move synchronous in opposite directions, the fiber can be kept on the central axis of the flow. This will be realized without displacement relative to the monitoring system during the stretching procedure that is described below. Each piezo actuator achieves a maximum motor velocity of 6 mm/s. As a result, the fiber could be elongated with rates between 0.10 and 12 mm/s. Furthermore, the maximum linear travel range of each motor is 11 mm with a minimum incremental motion of 8 nm. The maximum drive force is 0.6 N each piezo motor. The length of the clamped fiber between the two clamping points is 40 mm. Combined with the 11 mm travel range of each mounting stage (piezo motor) the fiber could be stretched with a maximum 22 mm (55% elongation), which is in its elastic range. Operation parameters for the stretching procedure in this study are the elongation rate at the fiber and the velocity of the airflow. In this study stretching and relaxation process were performed in a continuous mode. For further studies, it will be possible to vary the number of stretching cycles and perform a stretching procedure with periodically breaks.

2.4. Stretching set-up and stretching procedure

To observe the stretching of the loaded single fiber, the fiber-mount (see Fig. 6) was placed under a microscope (Wild Heerbrugg) using a xy-stage for precision positioning. During the stretching procedure, the fiber was exposed to a particle free airflow with a superficial flow velocity of less than 1 m/s. Air from the pressurized air supply line, expanded to ambient pressure, was used for the airflow, with a relative humidity of about 10% and a temperature of 25 °C. The airflow of particle-free air was shifted by 90° compared to the particle loading procedure. Direction of loading procedure corresponds to the line of sight during stretching. The fiber had to remain optically accessible from the top for observation (see Fig. 7 magnification of stretching area). Illumination of the fiber was installed in the opposite direction.

The loaded part of the fiber remained in the flow axis during the stretching procedure. The inlet pipe had a diameter of 16 mm. The distance between the inlet pipe and the elastic fiber was 10 mm. The flow passes a flow rectifier before reaching the fiber. The superficial flow velocity could be varied between 0.4 and 2 m/s. Image acquisition was performed with a microscope camera, a stable frame rate of 10 frames/s and a resolution of 3.1 MPixel. The grayscale of the video images was inverted during recording, resulting in light gray values for the fiber and deposited particle structure and dark gray values for the bright area of the illuminated background. In every experiment with an airflow, the loaded fiber was initially exposed to the airflow for 10 s before the stretching procedure started. (holding phase 1) Stretching was performed with an entire elongation of 22 mm (continuous stretching). In the state of maximum elongation, the fiber was retained for 60 s (holding phase 2). The airflow continued. Afterwards the fiber was relaxed back to the starting position applying the same movement parameters (continuous relaxation). After continuous relaxation, the fiber remained in the initial position for 10 s (holding phase 3).

Table 1 shows a detailed overview of stretching procedure data. All stretching procedures were performed under ambient pressure

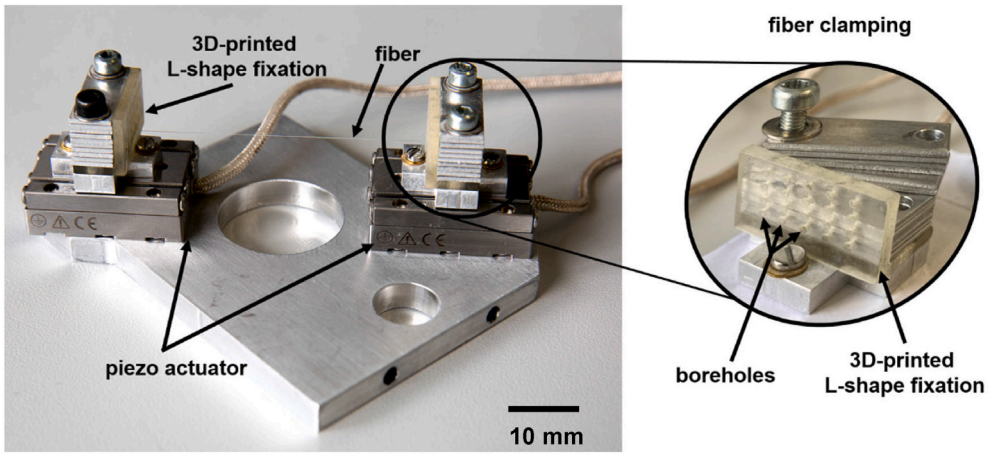

Fig. 6. Image of the designed fiber-mounting device for stretching the elastic fiber.

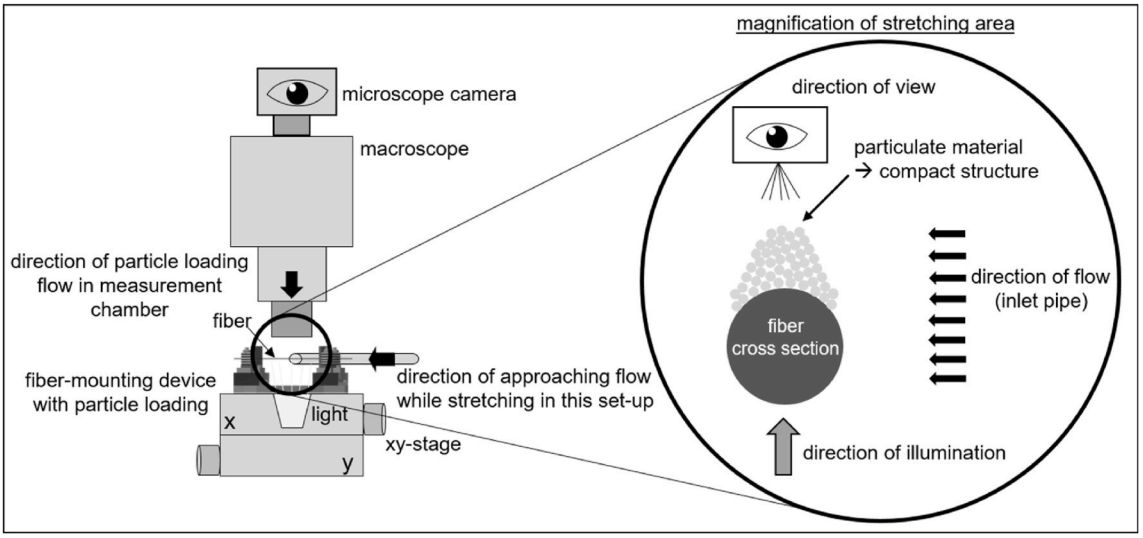

Fig. 7. Schematic set-up used for fiber stretching including the fiber-mounting device with loaded fiber and the microscope camera.

and temperature and without any housing of the fiber-mounting device.

2.5. Evaluation of experimental results and method of frame fitting

Stretching of the elastic filter fiber shall promote the formation of cracks and detachment of the PS fragments from the fiber. Besides the visual/qualitative observation of the fiber and the detachment of particulate material during the stretching process, a more quantitative analysis for different experiments can be established by comparing the projection area of successive frames in a video of critical section of the fiber (Zoller et al., 2020). An example is shown in Fig. 8. The projection area of bright pixels representing the particles on the fiber is reduced from one frame to the next. The progression of particle projection area is used as a measure for the effects that appear during fiber stretching.

As the detection area of the microscope camera is limited to the central section of the fiber, a part of the loaded fiber is moving out of the field of view while stretching the fiber. Consequently, there would be a loss of data during the stretching and relaxation process. This loss is eliminated by adapting the region of interest (ROI) of each frame according to the grabbed frame data respective fiber length.

This procedure is named “frame fitting”. During the holding phases, the size of ROI is constant between the frames within this phase. During the stretching or relaxation procedure, the ROI is increasing or decreasing among the frames. Fig. 9 shows an exemplary recorded frame including the frame fitting method. For the maximum elongation of the fiber, the length of the ROI in x-direction corresponds to the maximum length of the detected image of 2048 px. With the start of the stretching procedure, the ROI_{Start} is 1430 px. 440 px correspond to a length of 1 mm. Depending on the elongation length and the clamped length of the fiber, the increment ROI_{add} of the ROI has to be calculated. The size of the ROI is changed by adding gradually about the size of ROI_{add} on both side of the ROI of previous frame (see Fig. 9). When starting the relaxation of the fiber, the ROI is reduced again gradually in direction of x-axis down to 1430 px. Thus, for each frame, the ROI is fitted for the current stretching length.

Each frame of the obtained video material was processed with a MATLAB© procedure illustrated in Fig. 10. With the implemented image analysis, the projection area of loaded fiber for each moment of the experiment was calculated.

First, each frame is grabbed with its timestamp/frame data. Based on the frame data (stretching time, relaxing time or holding time) the size of region of interest (ROI) is determined. For a more accurate processing, each frame is converted to a MATLAB© grayscale image. Subsequently the image is binarized using the known method of Otsu (Otsu, 1979). Within the binarized image, the bright pixels are counted. Those represent the absolute projection area of fiber and particulate material on the fiber (PPA_i) on an initial fiber length of 4.65 mm.

Table 1
Data of stretching procedure.

step:	phase:	duration:
1	holding phase	10 s
2	continuous stretching	55 s (0.4 mm/s); 18.33 s (1.2 mm/s)
3	holding phase 2	60 s
4	continuous relaxation	duration: 55 s (0.4 mm/s); 18.33 s (1.2 mm/s)
5	holding phase 3	10 s

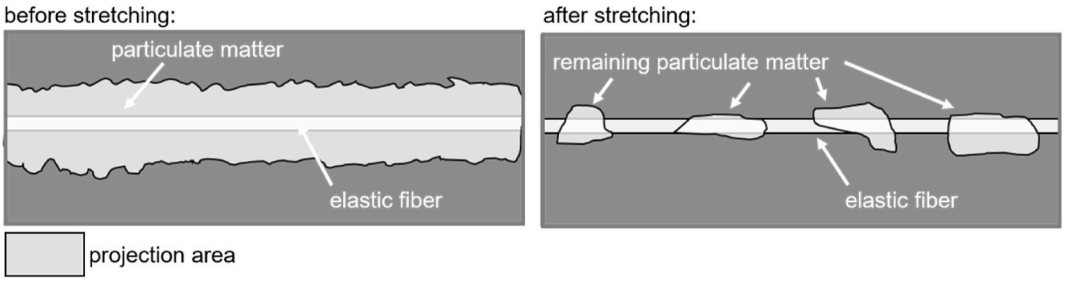

Fig. 8. Schematic illustrating the size of projection area of two consecutive frames when stretching the elastic fiber.

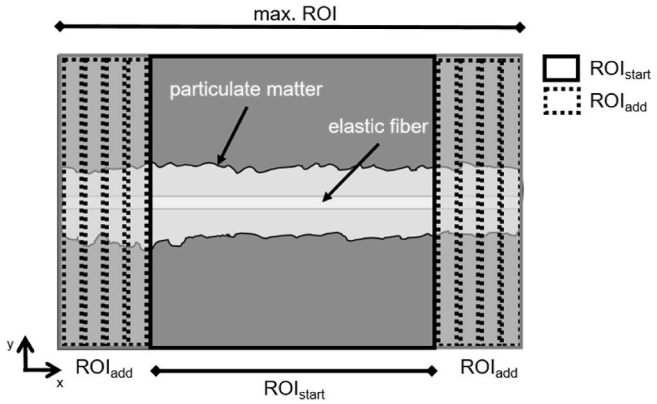

Fig. 9. Schematic of the changing size of the ROI. ROI is adapted for each frame separately before the image analysis.

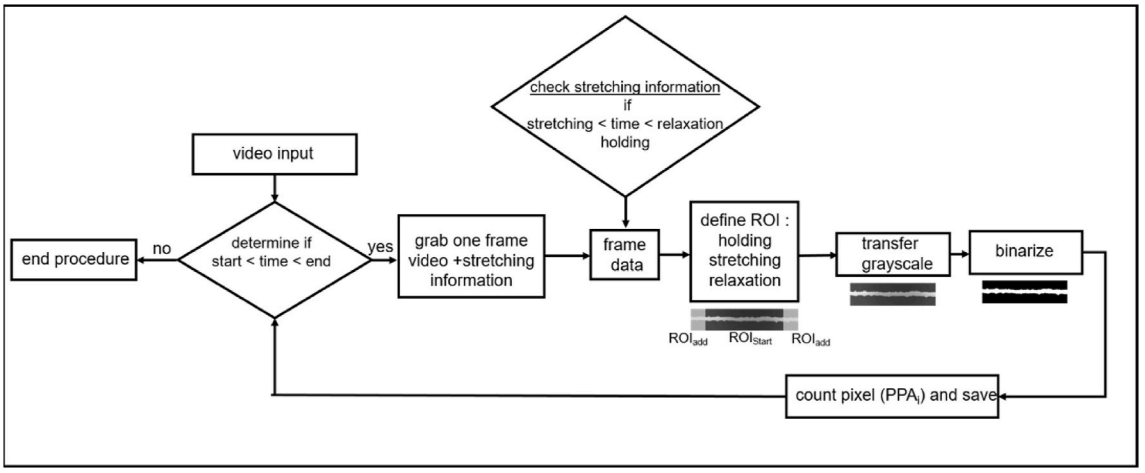

Fig. 10. Procedure for image analysis of the recorded data. Determine of PPA as an indicator for detachment and change in structure of the particle loading on the fiber.

For each experiment, the elastic fiber is newly loaded with particulate material. To observe repeatable behavior of the stretching process, a uniform compact deposition pattern was aspired. (Kanaoka et al., 1986; Kostoglou und Konstandopoulos 2000). Nevertheless, there are random variations of the particle projection area that result from small fluctuations during the particle deposition procedure in the measurement chamber. Therefore, the relative particle projection area (rPPA) was used to evaluate the change in particle projection area.

For the rPPA value of each frame, the current particle projection area of each frame PPA_i is set in relation to the initial particle projection area PPA_{Start} at the start of the stretching process (see Eq. (1)).

$$rPPA = \frac{PPA_i}{PPA_{Start}} \tag{1}$$

Effects such as the re-arrangement and rotation of the particle structures on the fiber can also contribute to changes – and generate artefacts – in the particle projection area (indirect rPPA). The rotation of the particulate structure is initiated by the internal twist and thus, torsion of the fiber. However, these events are detected by qualitative visual observation. The size of detached agglomerates cannot be determined due to the low framerate of the camera. A future step is to perform a more quantitative analysis of detached particle agglomerates by using an accurate measurement technique. This might gain more knowledge about the thickness/height of the particulate structures released from the fiber.

3. Results and discussion

3.1. Details on qualitative and quantitative data/combination with supplementary data

The results shown in the following will give a qualitative and a semi-quantitative overview of the effects occurring within the particle structure on the elastic fiber during the stretching process. Each of the experiments were performed threefold, including two replicate runs. The complete data is available in the supplement data section.

Currently, no exact quantification of the detached particle material is possible, so the analysis is limited to a descriptive report of the events on the fiber, as well as a partial quantification of the (residual) particle structure on the fiber by analyzing the particle projection area including rPPA. The size and height of detached particle fragments could give insight into the exact stress needed for first and multiple crack initiation (Nahta und Moran B. 1995).

An exact prediction based on time or elongation is currently not possible. Therefore, a first description of those effects based on repeated trials and a representative example seems reasonable.

3.2. Stretching without airflow

At first, the influence of fiber stretching on the behavior PS is investigated without an airflow ($v_s = 0$ m/s) to the fiber. Fig. 11 and Fig. 12 depict representative images of a loaded fiber during the stretching, holding and relaxing phases. Due to the used airflow velocity during the loading process, the PS on each fiber has a compact shape during the first holding phase and at the start of the stretching phase (see Fig. 11 I. and Fig. 12 I.).

Fig. 11 shows the fiber, which is stretched with an elongation rate of 0.4 mm/s. At the beginning of the stretching phase, the PS start

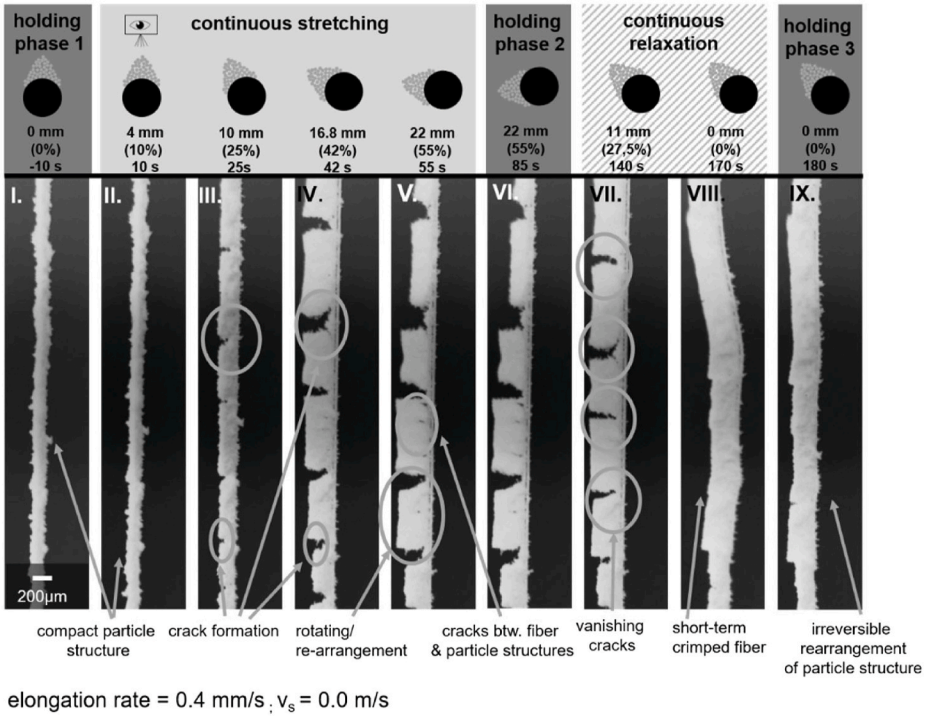

Fig. 11. Photographs (inverted) of the deposited particulates structure during one stretching and relaxation cycle of a particle loaded fiber. Without a superficial airflow. Elongation/contraction rate of 0.4 mm/s. Compact structure at the beginning. Above the images denoted: the elongation length of the fiber, the time of stretching experiment. Pictograms of the loaded fiber indicate the rotation of the fiber and the change in particle loading. No frame-fitting within this images.

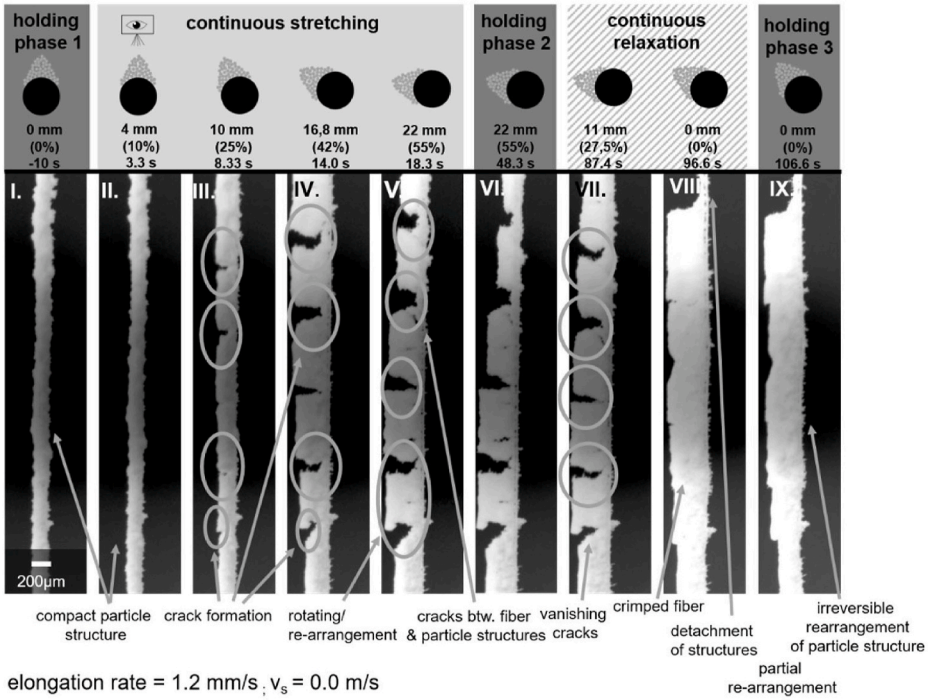

Fig. 12. Photographs (inverted) of the deposited particulates structure during one stretching and relaxation cycle of a particle loaded fiber. Without a superficial airflow. Elongation/contractions rate of 1.2 mm/s. Compact structure at the beginning. Above the images denoted: the elongation length of the fiber, the time of stretching experiment. Pictograms of the loaded fiber indicate the rotation of the fiber and the change in particle loading. No frame-fitting within this images.

to move and slide along with the fiber in direction of stretching. First crack formation within the compact PS is obtained at a total stretching length of 8 mm (36% stretching) (see Fig. 11 III.). In detail, the deposited particulate material starts to separate into structures on the fiber (inter-particle contact cracking) as supposed in Table 2. These structures have a size between 550 µm and 800 µm (in visible length). Due to the continuing stretching, the cracks between the separated PS fragments are increasing (see Fig. 11 IV.). Besides the crack formation, the fiber is rotating including the PS on the fiber, so the contact line between PS and fiber becomes visible

Table 2
Schematic of hypothesis on behavior of agglomerates and particles during fiber stretching.

mechanism	1. adhesion	2. slide	3. cracking	
			interparticle contact	particle contact to fiber
number of contact points to fiber	1	≥ 2		
1. fiber initial length				
2. fiber stretched		slipping/sliding	agglomerate breaks	contact point to fiber breaks; detachment
3. return to fiber initial length	remaining – no effects due stretching	remaining structure	re-arrangement	with residual particles

increasing particle load

(see Fig. 11 V.). In addition, the rotation of the fiber is shown schematically above the corresponding image of the fiber. At the end of the continuous stretching phase the crack formation and re-arrangement reaches its maximum (see Fig. 11 V.). During the second holding phase, the fiber stays elongated at 22 mm (55% stretching) for 60 s. Within the PS on the fiber, no change is visible in this phase (see Fig. 11 VI.). As the continuous relaxation starts, the emerged cracks start to vanish. The relaxation of the fiber is performed at a contraction rate of 0.4 mm/s. At the end of the relaxation process, the fiber is slightly crimped. The structure/form of the fiber re-generates gradually to straight cylinder line within 10 s after the end of the relaxation phase. As Fig. 11 IX. shows, the particle material on the fiber is in a compact shape again after the stretching procedure. The re-arrangement of the PS on the fiber and rotating of the fiber seems to be at least partially irreversible (see Fig. 11 IX). In total, fiber stretching at this elongation rate without airflow causes only re-arrangement and formation of cracks (see Table 2). Detachment of PS fragments was not observed. Further, the fiber is rotating around its axis. The rotation of the fiber is caused by the internal twist within the fiber.

To emphasize the first effects of the elongation rate, Fig. 12 shows representative images of the fiber that is stretched with a tripled elongation rate of 1.2 mm/s without an airflow. As seen before, the PS on the fiber has a compact shape in the beginning. First crack formation is obtained between a fiber elongation of 4 mm (10% stretching) to 10 mm (25% stretching). The broken up structures between the cracks have the same size as in the experiment with an elongation rate of 0.4 mm/s. With continuing stretching, the separate structures start re-arranging and the fiber, including the PS on the fiber, rotates around its axis. The presumed rotation of the fiber is shown in schematic images above each photograph of the fiber. During the second holding phase, PS fragments on the fiber re-arrange without stretching which is visible by the reduced bright area of the upper two PS segments in Fig. 12 VI. Further, within the separated PS fragments on the fiber, cracks emerged during the last millimeter of the continuous stretching phase. In comparison to the experiment with the elongation rate of 0.4 mm/s re-arrangement and fiber rotation is more distinctive with an elongation rate of 1.2 mm/s. At the start of the continuous relaxation phase, the fiber including the PS fragments seem to rotate back to their initial position. As shown in Fig. 12 VII. the cracks start vanishing with decreasing fiber elongation. As a single event, detachment of a small PS could be observed in Fig. 12 VIII. Back to initial fiber length, the cracks within the total PS on the fiber have vanished. However, it becomes obvious that an irreversible re-arrangement of PS fragments on the fiber took place. Some rotation of the PS segments is still visible at the upstream contour of the PS on the fiber. Comparing to the experiment with the elongation rate of 0.4 mm/s the fiber is less crimped. During the third holding phase, the slight crimp of the fiber is slowly vanishing. As Fig. 12 IX. shows, the particle material on the fiber is still in the compact shape after the stretching procedure. Similar to in the experiment with a lower elongation rate of 0.4 mm/s, the fiber stretching mainly promote crack formation and rotation of the fiber including the PS on the fiber. However, during the relaxation phase, first detachment of PS has been observed. The stretching of the fiber might weaken the PS and their contact to the fiber, so small parts detach during the relaxation procedure. A schematically overview of this mechanism was given in Table 2.

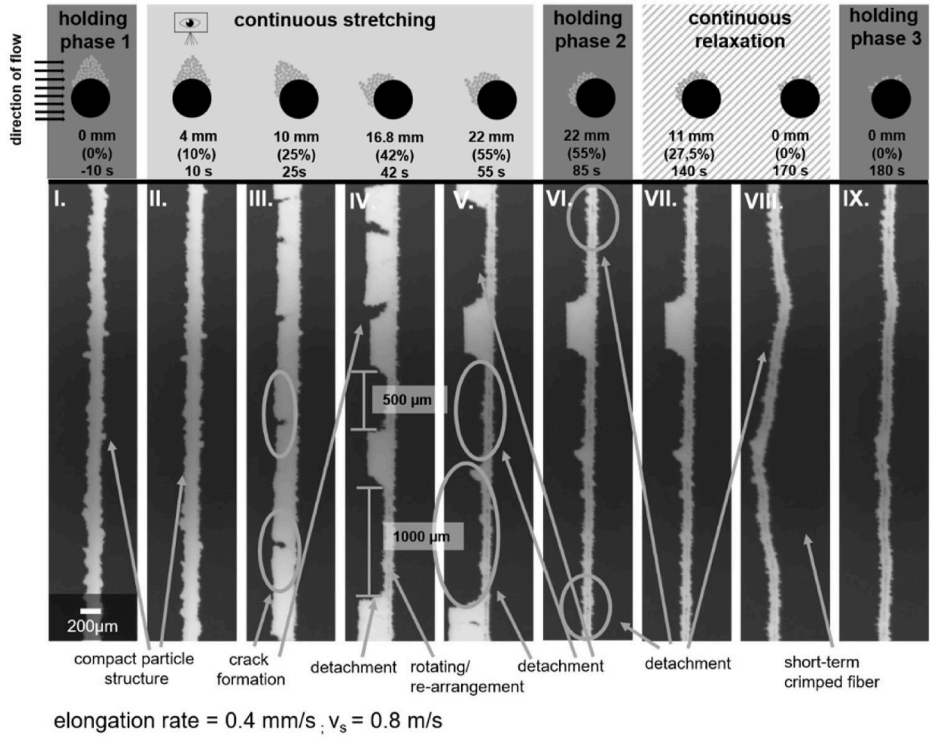

Fig. 13. Photographs (inverted) of the deposited particulate structure during one stretching and relaxation cycle of a particle loaded fiber. With a superficial airflow of 0.8 m/s. Compact PS on the fiber at the beginning. Above the images denoted: the elongation length of the fiber, the time of stretching experiment. Pictograms of the loaded fiber indicate the rotation of the fiber and the change in particle loading. No frame-fitting within this images.

3.3. Stretching with airflow

In the experiment without an airflow, detachment of PS fragments does not occur by just stretching a single fiber slowly. Hence, the fiber is exposed to an additional airflow (as indicated in the images from the left side) at a superficial velocity of 0.8 m/s while beginning stretching at an elongation rate of 0.4 mm/s. Fig. 13 depicts representative images of the fiber during the different phases. During the first holding phase, the loaded fiber is just exposed to an airflow of 0.8 m/s for 10 s. Fig. 13 I. shows no particle detachment or re-arrangement occurs during this phase. As shown in Fig. 13 II. the PS on the fiber maintains in a compact shape during the first 4 mm (10% stretching) of elongation. After 6 mm (15% stretching) of continuous stretching first cracks emerge in the PS on the fiber. The formation of cracks increases with the increasing elongation length (see Fig. 13 III. after 10 mm (25% stretching) of stretching). The whole PS might slide on the fiber. In addition, the fiber is rotating and the PS re-arrange on the fiber as already observed in experiments without an airflow. In this experiment the rotation of the fiber was in the same direction that had been observed in the experiment before without an airflow. The emerging cracks seem to have the same size and spacing as well. The residual obtained PS fragments are rotated into the direction of airflow (luv side of the fiber). First detachment of PS fragments from the fiber occurred at an elongation of 10.8 mm (27% stretching). At once the rotation of the fiber and the re-arrangement of PS fragments on the fiber proceeds. The first detached PS fragments have a size between 500 and 1000 µm. At the end of the stretching phase (after 18.33 s), a large part of the PS is already detached from the fiber (see Fig. 13 V.). The fiber rotating and re-arrangement/orientation of agglomerates to the luv side of the fiber does not inhibit detachment. As Löffler obtained, particulate material is more likely to detach in bigger PS fragments (piles) from the fiber than just single particles (Löffler, 1972). Starting the second holding phase between the continuous stretching and continuous relaxations procedure some PS fragments detach from the fiber (see at the side of the photographs). Fig. 13 VI. shows that some residual single particles remained on the fiber in areas where big PS fragments detached. During the second holding phase, the fiber is still rotated as seen in the schematics above the images of the fiber. Within the continuous relaxation phase, the remaining part of PS detached from the fiber. The fiber starts crimping as depicted in Fig. 13 VIII. During the third holding phase, the short-term crimped fiber is straightened back to initial state.

In order to quantify the phenomena on the fiber, the rPPA, instead of qualitative images of the stretching experiments, were investigated. Fig. 14 shows the recorded rPPA during the stretching processes without and with a superficial airflow to the fiber. The elongation rate in both cases was 0.4 mm/s. The continuous data is divided in five sections in accordance to the steps during the stretching procedure as described in section 2.4. In both experiments without and with an airflow, the rPPA remains on a constant level during the first holding phase of 10 s. No PS fragments re-arrange or detach. The fiber including the PS is not rotated yet, as indicated by the pictograms. For the experiment without an airflow (black line) the rPPA starts increasing after 5 mm (12.5% stretching) of stretching. rPPA increases continuously because the fiber is rotating around its axis (as indicated by pictogram) in combination with re-

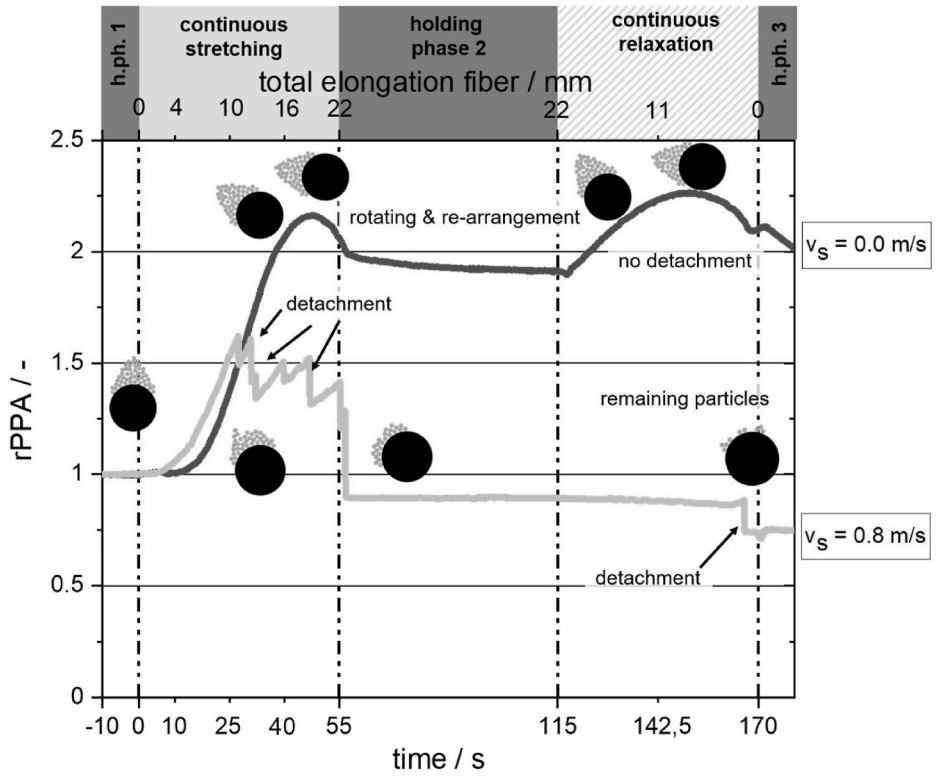

Fig. 14. rPPA plotted versus elongation and time during the stretching and relaxing procedure without and with an airflow. Constant elongation/contraction rate of 0.4 mm/s. The pictograms indicate the rotation of the fiber and detachment phenomena occurring on the fiber like in Figs. 11 and 13.

arrangement and sliding of the PS fragments on the fiber. Maximum of rPPA is reached almost at the end of the elongation. A decrease of rPPA is based on the rotating PS fragments that are leaving the observation level. During the second holding phase of 60 s the rPPA is decreasing slightly due to the re-arrangement of PS fragments. In general, the rPPA is remaining on a value of almost twice the initial value. Starting the relaxation phase after the second holding phase, the rPPA is increasing again because the cracks within the PS on the fiber start vanishing. By reaching the initial state of the fiber length, the rPPA is still on a level way above the starting level. The elastic fiber is crimped at the end of the relaxation process (see Fig. 11 XII.). Remaining PS fragments on the fiber have been re-arranged irreversible and remain in the position they had during the second holding phase. These appearances are reasons for the rPPA above 1. During the holding third holding phase the crimp of the fiber is vanishing, but the re-arrangement of PS fragments on the fiber remains. In total, the rPPA of the fiber is increasing above the initial level of 1 during the five phases of the experiment. There was no significant and sudden decrease of the rPPA during the whole experiment, which would be an indicator for detachment of particles.

In the experiment with an airflow of 0.8 m/s (see Fig. 14 gray line) the rPPA starts increasing after 2.5 mm (6.25% stretching) of stretching. rPPA is rising continuously with the continuing elongation of the fiber. The fiber is rotating around its axis and the PS is re-arranging to the luv side of the fiber. The rPPA reaches its maximum almost in the middle of the stretching phase. First detachment of particles is indicated by a sudden decrease of rPPA at an elongation of 10.8 mm (27% stretching). Moreover, up to the maximum stretching length of the fiber the rPPA is decreasing significantly multiple times. These events are linked to further detachment of PS fragments from the fiber (see Fig. 13 IV. and V.). Reaching the maximum of the elongation length the rPPA is below the initial level at the start of the experiment. During the second holding phase between stretching and relaxation phase, there is no change in the rPPA. The fiber including the residual PS on the fiber is remaining in the rotated state as indicated by the pictogram. During the continuous relaxation phase, the rPPA is remaining on the same level as during the holding phase, except a small decrease at the end, which is linked to detachment of PS fragments from the fiber. The fiber is crimped after reaching the initial elongation. The rPPA level is remaining constant because there are no more PS fragments on the fiber that could rotate or influence the particle projection area.

Comparing the experiments with and without an airflow it was obtained that PS fragments just detach in the combination of stretching of 0.4 mm/s and an airflow. The stretching procedure might induce shear and tensile stress leading to cracking within particle-structures and between fiber and particle-structures (see Table 2). Thus, the PS fragments are more likely to re-arrange and finally detach if exposed to an airflow. In all corresponding repeated experiments, the same phenomena of re-arrangement, rotation and detachment could be observed (see supplementary data). In both cases, the PS fragments might slide and rotate on/with the fiber before the cracking.

3.4. *Impact of different airflow velocities on the detachment behavior of particle structures on the fiber*

To illustrate the influence of the superficial airflow velocity on the behavior of PS on the fiber, Fig. 15 shows representative images of the loaded fiber exposed to three different airflow velocities. The applied airflow velocities are 0.4 m/s, 0.6 m/s and 0.8 m/s

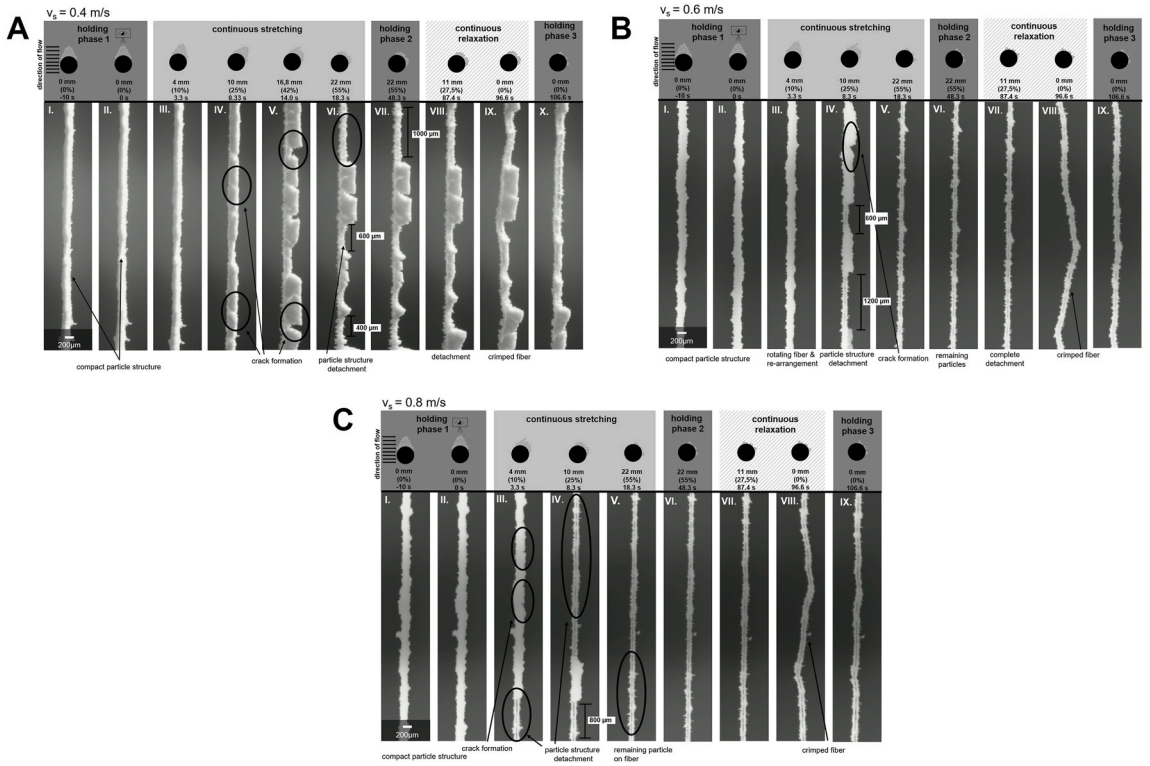

Fig. 15. Photographs (inverted) of the loaded fiber during detachment experiments with a constant elongation/contraction rate of 1.2 mm/s and various superficial velocities of the airflow. a) 0.4 m/s, b) 0.6 m/s, c) 0.8 m/s.

respectively. For reasons of comparisons, one of the airflow velocities is the same as in the experiments above. Direction of airflow is from the left side as indicated in each figure. In every experiment, the elongation rate was 1.2 mm/s. The fiber is exposed to the airflow (at its velocity v_s) during the entire experiment. All experiments were repeated two times. The video material of each individual experimental run can be found in the supplementary data.

During the first holding phase of each experiment, the particle loaded fiber is just exposed to the airflow. As shown in the images in Fig. 15 a) b) c) I., the PS on the fiber has the desired compact shape at the begin of the experiments. Further, no detachment occurs in any experiment during the first 10 s without stretching the fiber (see Fig. 15 a) b) c) II.). This confirms the findings of Löffler (Löffler, 1972) that no detachment of PS fragments occurs at these airflow velocities below 1 m/s. Fig. 15 a) depicts representative images of a fiber during one stretching procedure at an airflow velocity of 0.4 m/s. First crack formation and re-arrangement of the PS fragments is observed at a fiber elongation of 9 mm (22.5% stretching) (see Fig. 15 a) IV.). Formation of cracks is intensifying during the continuous stretching phase. Starting the stretching process the fiber also begins to rotate around its axis. The rotation of the fiber is indicated by the pictogram above the fiber images. The fiber rotates to the far side of the airflow (lee side of the fiber). As shown in the images, the particulate structures follow the movement of the fiber. First detachment of PS fragments was observed at a fiber elongation of 19.2 mm (48% stretching). The detached PS fragments have a size between 400 μm and 1000 μm. During the second holding phase, no further PS fragments detached from the fiber. During the relaxation phase of the fiber, the cracks within the PS on the fiber start vanishing. The PS fragments re-arrange on the fiber. As shown in Fig. 15 a) X. the shape of the visible projected PS is completely changed comparing to the start of fiber stretching (see Fig. 15 a) II.). A layer of residual particles is left on the fiber. Further, the fiber is crimped at the end of the relaxation phase. During the third holding phase, some big PS fragments detach from the fiber. The PS fragments might have been loosened by the stretching and relaxation procedure. As observed before some residual particle remained on the fiber at the end of the third holding phase (see Table 2, detachment with residual particle).

Increasing the airflow velocity up to 0.6 m/s first detachment of PS fragments occurred at a fiber elongation of 9.6 mm (24% stretching). As shown in Fig. 15 b) IV. the formation of cracks and re-arrangement was not that pronounced as at airflow velocities of 0.4 m/s. The first detached PS fragments have a size up to 1200 μm. In Fig. 15 b) IV. crack formation and rotation of the fiber is visible. At the end of the continuous stretching phase, a huge amount of PS fragments detached from the fiber. Single particles and small residual PS fragments are remaining on the fiber (see Fig. 15 b) V.). During second holding phase and the relaxation phase, no further particle detachment is observed. As shown in Fig. 15 b) VIII. the fiber is crimped after the relaxation phase. No particles detach during the disappearing of fiber crimp in holding phase 3 (see Fig. 15 b). IX.)

Fig. 15 c) depicts representative images of the fiber during the stretching procedure exposed to an airflow of 0.8 m/s. First detachment of PS fragments was observed at a fiber elongation of 3.6 mm (9%). Crack formation and rotation of the fiber preceded the detachment of PS fragments. The rotation of the fiber is shown by the pictograms. The piles on the fiber seem to orientate to the lee side of the fiber. As observed before, the fiber is rotating around its axis, too. At an elongation of 10 mm (25% stretching) almost the complete PS is detached from the fiber. As indicated in Fig. 15 c) IV. the size of the PS fragment is around 800 μm. At the end of the continuous stretching phase, there are just single particles and small agglomerates remaining on the fiber. No detachment of small PS fragments occurred during the second holding phase and the relaxation phase. The bond between single particles and the fiber appears to be more resilient than the adhesion force within the PS. As observed before during the experiments at different superficial airflow velocities, the crimp of the fiber disappears within the 10 s after the end of the relaxation phase.

For a more quantitative and continuously analysis of the phenomena on the fiber, instead of qualitative single images of the representative stretching experiments, the rPPA could be investigated. Fig. 16 shows the recorded rPPA during the stretching processes for the experiments at three different superficial airflow velocities including an experiment without an airflow (light gray dotted line, $v_s = 0$ m/s). The fiber is elongated in all experiments with an elongation rate of 1.2 mm/s.

In all experiments, the rPPA is remaining at the initial level in holding phase 1. No PS fragments re-arrange or detach on/from the fiber just by the airflow without stretching. During the first 1 mm (2.5% stretching) of stretching, the rPPA of all experiments is remaining at the initial level. After an elongation of 1 mm (2.5% stretching) the rPPA in the experiment with superficial airflow velocity of 0.6 m/s and 0.8 m/s respectively are increasing until the first PS fragments detached from the fiber. The increase of rPPA is based on the re-arrangement of PS fragments and the rotation of the fiber that is depicted by the pictograms. The largest increase of rPPA is observed at an airflow velocity of 0.4 m/s and in the experiment with no airflow ($v_s = 0$ m/s). PS fragments have more time to re-arrange on the fiber and the formation of cracks is more distinctive (see representative images Figs. 15 a) and Fig. 12). Detachment of PS fragments is characterized by a sudden decrease of rPPA. For all experiments, the rPPA is increasing above 1 during the first seconds of stretching phase. By detachment of agglomerates during the continuous stretching phase, the rPPA is decreasing below 1 for the experiment at superficial airflow velocities of 0.6 m/s and 0.8 m/s. In both experiments, not further significant change in rPPA could be observed because all particles detached from the fiber. In the experiment with an airflow velocity of 0.8 m/s first detachment occurs at an elongation of 4 mm (18% stretching). In the experiments with lower airflow velocity (0.6 m/s and 0.4 m/s), first detachment occurs only at an elongation of 9.6 mm (24% stretching) and 19.2 mm (48% stretching) respectively. In the experiment with $v_s = 0.8$ m/s and $v_s = 0.6$ m/s almost all particle detach during the first half of the continuous stretching phase. The rPPA of the experiment at a superficial airflow velocity of 0.4 m/s is remaining on a constant level above 1 in the second holding phase. This is caused by increased irreversible re-arrangement of PS fragments and rotation of the fiber. Further, a large part of PS is remaining on the fiber. The slight change in rPPA during the relaxation phase is based on fiber rotation and re-arrangement of the PS on the fiber. During the third holding phase, there is a sudden decrease, which is linked to detachment of PS fragments. The connection between PS on the fiber and the fiber might degrade by the stretching and relaxation procedure, so PS detachment gets more likely (see Table 2).

In the experiment without an airflow, the decrease of rPPA at the end of continuous stretching phase is less abrupt. PS fragments re-arrange and rotate on the fiber. During the second holding phase, this process continues without any external influences. By the start of

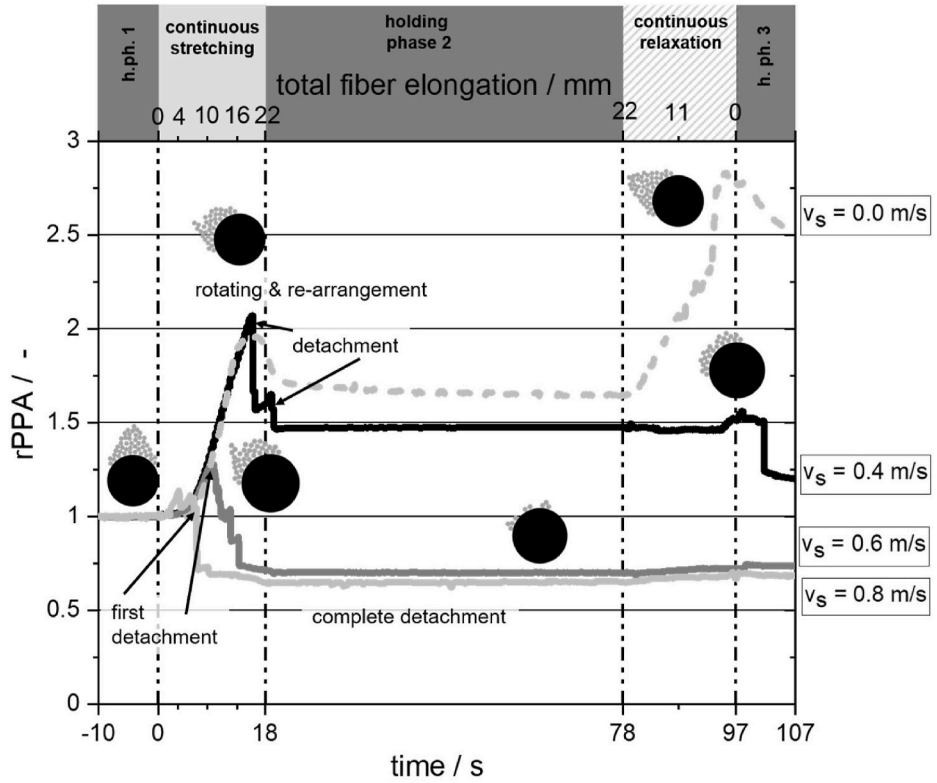

Fig. 16. rPPA of stretching experiments with different superficial airflow velocities and one elongation/contraction rate of 1.2 mm/s.

the relaxation, the rPPA is increasing again due to the rollback of crack formation. A sudden decrease of rPPA at the beginning of the third holding phase is linked to more intensified rotation/re-arrangement and detachment of small PS fragments. In comparison to the experiment with an airflow, the rPPA is above the initial level that results from an irreversible change in PS on the fiber and almost no detachment of PS fragments.

3.5. Hypothesis concerning behavior of particle structures on elastic single fiber during stretching based on the observation/crack formation in matrix on elastic substrate

Resulting from the qualitative observations during the stretching experiments, Table 2 summarizes potential applicable mechanisms for the sliding, re-arrangement, cracking and detachment of spherical particles and agglomerates under fiber-stretching conditions. There are three potential mechanisms of behavior of PS fragments on an elastic fiber based on the fundamental idea of the movement of the substrate beneath a particulate structure. (Soltani und Ahmadi 1994) All of them depend on the geometry of the contact and the cohesive/adhesive forces of the particulate deposit.

One determining parameter for the different mechanisms is the number of contact points to the fiber. A single spherical particle has only one fiber contact point whereas agglomerates of particles have higher numbers of fiber contact points. Single particles with one contact point to the fiber might adhere to the fiber while it is stretched. For agglomerates or a contiguous area, fiber stretching induces stress to the particle structure and thus, can result in sliding and cracking of structures. Detachment is a result of complete contact point breakage between agglomerates and the elastic fiber or/and between neighboring agglomerates/particles. Based on the first observations in the experiments shown, residual particles always remain on the fiber, after detachment of agglomerates from the fiber. The theoretical breaking stress of a particle structure can be calculated according to Rumpf and Hamaker (HC Hamaker, 1937; Rumpf, 1970). For the determination of the force between fiber and particle structure, normally the deformation of the substrate must be taken into account. According to Schütz and Schubert, this contribution is negligible in case of calculation of adhesion force for e.g. limestone particle and silver steel plate (Schütz und Schubert 1976; Schubert, 1979). In the case of elastic materials, discarding this deformation might not be valid and could give an explanation for the residual particles. All mentioned processes are potentially preceded by a change in number of contact points. Further, a crossover of mechanisms of PS fragments behavior is imaginable.

A relevant factor for detachment and cracking effects is the analysis of the applied tension on the fiber (substrate) and the matrix on the fiber. If the induced stress σ exceeds a critical value σ^*, the first fracture occurs within the matrix on the elastic substrate. (Nahta und Moran B. 1995) Cracking of the particle structure on the fiber was observed in all shown experiments. Schematic of film/substrate system with cracking is shown in Fig. 17.

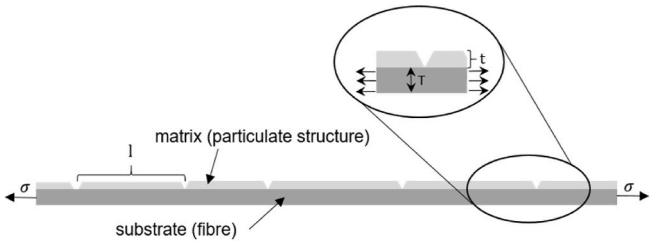

Fig. 17. Schematic of the stress model on a plane substrate covered with a matrix layer. Applied stress to the substrate. Modified from (Nahta und Moran B. 1995).

Thouless and Beuth have carried out fundamental investigations on the factors influencing this initiation stress for crack (Beuth, 1992; Thouless, 1990). The height t of the thin film (particle structure) is crucial. Further, the length l of the particle fragments is characteristic for the applied or induced stress of the substrate beneath. This results in an energy release rate at the tip of each crack, which is able to grow further in the matrix/film. The rate is given in Eq. (2).

$$G_m(l/t,\ \sigma) = \frac{\sigma^2 \pi z (1-\nu^2)}{E} F(s)^2 \tag{2}$$

The correlation of G_m includes the Young's modulus E of the substrate (fiber), as well as the applied stress σ during initial cracking and the Poisson's ratio ν of the substrate. Moreover, the exact depth z and length of the cracks is needed for the function F(s) shown by Thouless (Thouless, 1990). In addition to the influencing factors mentioned, a distinction is also made between the two cases of cracking without and with detachment of the matrix from the substrate (Nahta und Moran B. 1995).

Further accurate measurements of the height of the particle structure and the size of detached agglomerates will provide more information about the factors influencing detachment and cracking of the matrix (particle structure on the fiber). So far, the insights gained on the cracking process are the first introductory step to the understanding of the weakening of particle structure adhesion on the fiber, which ultimately leads to the detachment of the particle structures from the fiber. In addition to that, the applied airflow has a considerable influence on the detachment of particulate structures from the fiber, as drag forces create additional stress in the fracture zone. In each experiment with an applied airflow, particle structures detached from the fiber. The orientation of the particle structure, whether lee or luv to the fiber may have an influence on the detachment behavior as the exposed area of the particle structure is changed. Besides cracking of the particulate matrix, the stretching of the fiber is causing a tension in the fiber. The rotation of the fiber including the particulate material is caused by a torsion of the fiber. The torsion of the fiber is a result of the applied tension by stretching the fiber. However, due to a number of influencing variables which are currently unclear (e.g. the angle of fiber rotation), a precise estimation and modeling is difficult and not feasible yet.

4. Conclusion and outlook

The fundamental influence of the fiber stretching process on re-arrangement and detachment behavior of PS fragments on/from an elastic single fiber while exposure to gas flow is presented in this study. Before the stretching process, the fiber was loaded in a loading chamber with a defined compact PS. The compact morphology was obtained by a filtration velocity of 1.2 m/s under the given parameters of particle size distribution and fiber diameter, based on the findings of (Kanaoka et al., 1986) and (Kasper et al., 2010). To separate of the influence of the process parameters during stretching, some initial fiber stretching experiments were examined without an airflow. In subsequent experiments, the particle-loaded fiber was exposed to a particle free airflow during stretching. The observation and evaluation of the loaded fiber was examined with a microscope. Subsequent offline image analysis was realized by a MATLAB® routine. The main results are:

- A custom-designed fiber-mounting for investigations on loaded elastic filter fibers was constructed and applied for the first time.
- A method for image analysis of particle-projection area with an implemented frame fitting method to compensate for ROI growth during stretching was developed.
- At experiments with a low elongation rate below 1.2 mm/s and no airflow, no detachment of PS fragments from the fiber occurred in these experiments.
- In all experiments cracking of particulate structure on the fiber could be initiated by stretching the fiber
- PS fragments detach with the combination of a superficial airflow velocity below 1 m/s and an elongation rate of the fiber of at least 0.4 mm/s.
- Comparing to results for "conventional" fibers (Löffler, 1972) the dynamic/elastic fiber initiates PS detachment at reduced superficial airflow velocities below 1 m/s.
- Comparing to results of Zoller et al., piles of glass particles detached at velocities of 0.4 m/s with previous mechanical weakening of the particle structure instead of weakening by reaction (Zoller et al., 2020).
- Comparing to results of Jankowska et al. the surface and structure has a huge influence on the detachment/re-entrainment of particle and particle structure (Jankowska et al., 2000).

- PS re-arrangement combined with increasing rPPA occurred more frequently at lower elongation rates below 1.2 mm/s and without airflow.
- PS detachment is getting more likely with increasing airflow velocity at a constant elongation rate of 1.2 mm/s.
- Uncontrolled rotation/torsion of the fiber (internal twist) while stretching the fiber was observed independent of airflow.
- Rotation of the fiber causes re-orientation of piles luv and lee of the fiber

A more precise method for PS fragments analysis will be part of our future work in this field. A laser-sheet measurement technique in combination with an image analysis will be applied for detection and accurate size measurement of detached PS fragments. These investigations might result in more detailed analysis of the correlations between particle load, the applied process parameters and the probability of detachment. Moreover, an investigation of various multi-fiber configurations using a 3D-printed L-shaped fixation is possible, e.g. an arrangement of several fibers stacked or parallel.

The use of elastic fibers in filter media might be an enabler for adaptive filter systems in the future. These potential adaptive systems will have the aim to delay increasing filter backpressure while maintaining a high level of separation efficiency. Consequently, this could extend the loading capacity and life span of the filter.

Declaration of competing interest

The authors declare that they have no known competing financial interests or personal relationships that could have appeared to influence the work reported in this paper.

Acknowledgement

We gratefully acknowledge that this project was funded by the Deutsche Forschungsgemeinschaft (DFG, German Research Foundation) – 427981860.

We kindly thank Prof. Dr.-Ing. Peter Elsner, Dr.-Ing. Wilfried Liebig and Dr. -Ing. Jonas Huether from the Institute for Applied Materials (IAM), KIT, for use of their single fiber tensile test stand. We also kindly thank Freudenberg Filtration Technologies SE & Co. KG for donating fiber material to this research.

Appendix A. Supplementary data

Supplementary data to this article can be found online at https://doi.org/10.1016/j.jaerosci.2021.105785.

Graphics program

PowerPoint, Gimp.

References

Beuth, J. L. (1992). Cracking of thin bonded films in residual tension. *International Journal of Solids and Structures, 29*(13), 1657–1675. https://doi.org/10.1016/0020-7683(92)90015-L

Brown, R. C. (1993). *Air filtration. An integrated approach to the theory and applications of fibrous filters*. Oxford: Pergamon Press Ltd.

Hamaker, H. C. (1937). The London—van der Waals attraction between spherical particles. *Physica, 4*, 1058–1072. https://doi.org/10.1016/S0031-8914(37)80203-7. Online verfügbar unter.

Jankowska, E., Reponen, T., Willeke, K., Grinshpun, Sergey, A., & Choi, K.-J. (2000). Collection of fungal spores on air filters and spore reentrainment from filters into air. *Journal of Aerosol Science, 31*, 969–978.

Kanaoka, C., Emi, H., Hiragi, S., & Myojo, T. (1986). Morphology of particulate agglomerates on a cylindrical fiber and a collection efficiency of a dust loaded fiber. In *Aerosols: Formation and reactivity 2nd aerosol conf. Berlin* (pp. 674–677).

Kanaoka, C., & Hiragi, S. (1990). Pressure drop of air filter with dust load. *Journal of Aerosol Science, 21*, 127–137.

Kasper, G., Schollmeier, S., & Meyer, J. (2010). Structure and density of deposits formed on filter fibers by inertial particle deposition and bounce. *Journal of Aerosol Science, 41*(12), 1167–1182. https://doi.org/10.1016/j.jaerosci.2010.08.006

Kostoglou, M., & Konstandopoulos, A. G. (2000). Particulate deposit shape evolution on cylinders in cross flow at high Stokes numbers. *Journal of Aerosol Science, 31*, 427–436.

Larsen, R. I. (1958). The adhesion and removal of particles attached to air filter surfaces. *American Industrial Hygiene Association Journal, 19*.

Löffler, F. (1972). Abblasen von an Filterfasern abgeschiedenen Feststoffteilchen. *Verfahrenstechnik, 6*, 3–7.

Lowden, R. A., & Stinton, D. P. (1988). Interface modification in Nicalon®/SiC composites. *Ceramic Engineering and Science Proceedings, 9*, 705-122.

Maus, R., & Umhauer, H. (1996). Collection and adhesion efficiency of biological particles on single fibers. *Journal of Aerosol Science, 27*.

Müller, T. (2017). *Trägheitsabscheidung von Partikeln an parallelen faserarrays. München: Dr. Hut (verfahrenstechnik)*.

Nahta, R., & Moran, B. (1995). Crack spacing in brittle films on dissimilar planar and axisymmetric elastic substrates. *Engineering Fracture Mechanics, 52*, 513–524.

Ochiai, S., & Murakami, Y. (1981). Theoretical prediction of tensile strength of fibers as a function of thickness of brittle zones on fiber surfaces. *Metallurgical Transactions A, 12A*, 1155–1161.

Otsu, N. (1979). A threshold selection method from gray-level histograms. *IEEE Trans. Syst., Man, Cybern, 9*(1), 62–66. https://doi.org/10.1109/TSMC.1979.4310076

Payatakes, A. C., & Gradoń, L. (1980). Dendritic deposition of aerosol particles in fibrous media by inertial impaction and interception. *Chemical Engineering Science, 35*, 1083–1096.

Payet, S., Boulaud, D., Madelaine, G., & Renoux, A. (1992). Penetration and pressure drop of HEPA Filter during loading with submicron liquid particle. *Journal of Aerosol Science, 23*, 723–735.

Przekop, R., Grzybowski, K., & Gradoń, L. (2004). Energy-balanced oscillatory model for description of particles deposition and Re-entrainment on fiber collector. *Aerosol Science and Technology, 38*(4), 330–337. https://doi.org/10.1080/02786820490427669

Qian, Y., Willeke, K., Ulevicius, V., & Grinshpun, S. A. (1997). Particle reentrainment from fibrous filters. *Aerosol Science and Technology, 27*(3), 394–404. https://doi.org/10.1080/02786829708965480

Rembor, H.-J., Maus, R., & Umhauer, H. (1999). Measurements of single fibre efficiencies at critical values of the Stokes number. *Particle & Particle Systems Characterization, 16*, 54–59.

Rumpf. (1970). Zur Theorie der Zugfestigkeit von Agglomeraten bei Kraftübertragung an Kontaktpunkten. *Chemie Ingenieur Technik, 42*, 538–540.

Schubert, H. (1979). Grundlagen des Agglomerierens. *Chemie Ingenieur Technik, 51*, 266–270. https://doi.org/10.1002/cite.330510404. Online verfügbar unter.

Schütz, W., & Schubert, H. (1976). Der Einfluß von Anpreßkräften auf die Partikelhaftung. *Chemie Ingenieur Technik, 48*, 567.

Schweers, E., Umhauer, H., & Löffler, F. (1994). Experimental investigation of particle collection on single fibres of different configurations. *Particle & Particle Systems Characterization*, 275–283.

Soltani, M., & Ahmadi, G. (1994). Particle removal mechanisms under substrate acceleration. *The Journal of Adhesion, 44*(3), 161–175. https://doi.org/10.1080/00218469408027075

Song, C. B., Park, H. S., & Lee, K. W. (2006). Experimental study of filter clogging with monodisperse PSL particles. *Powder Technology, 163*(3), 152–159. https://doi.org/10.1016/j.powtec.2006.01.016

Thomas, D., Penicot, P., Contal, P., Leclerc, D., & Vendel, J. (2001). Clogging of fibrous filters by solid aerosol particles Experimental and modelling study. *Chemical Engineering Science, 56*, 3549–3561.

Thouless, M. D. (1990). Crack spacing in brittle films on elastic substrates. *Journal of the American Ceramic Society, 73*, 2144–2146.

Wang, Q., Lin, X., & Chen, D.-R. (2016). Effect of dust loading rate on the loading characteristics of high efficiency filter media. *Powder Technology, 287*, 20–28. https://doi.org/10.1016/j.powtec.2015.09.032

Zoller, J., Zargaran, A., Braschke, K., Meyer, J., Janoske, U., & Dittler, A. (2020). Experimental investigation of reactive-inert particulate matter detachment from metal fibres at low flow velocities and different gas temperatures. *Aerosol Sci Eng*. https://doi.org/10.1007/s41810-020-00081-3